Metals and Materials International (2020) 26:1134–1143
https://doi.org/10.1007/s12540-019-00367-3

Mechanical Properties Improvement of Al–Li 8090 Alloy by Using the New Proposed Method of Directional Quenching

S. Nouri[1] · S. Sahmani[1] · M. Hadavi[2] · Sh. Mirdamadi[3]

Received: 28 January 2019 / Accepted: 7 July 2019 / Published online: 25 July 2019

Abstract
Due to having low density as well as high specific modulus and fatigue toughness, Al–Li alloys have been targeted as an advanced material for using in aerospace applications. In the current investigation, a new heat treatment method namely as directional quenching process is proposed to improve the mechanical properties of the Al–Li 8090 alloy, the results of which are compared with those of T6 and T8 aging heat treatment techniques. For this purpose, aging process at 170 °C is conducted in all of the three heat treatment methods, but the solutionizing treatment and quenching are performed along a specific direction in the introduced directional quenching method. The mechanical properties and fracography of cross-sectional fracture pattern of the heat treated samples are studied corresponding to the various heat treatments. Based on the obtained results, it is found that in comparison with the two conventional T6 and T8 heat treatment methods, the proposed directional quenching technique has the capability to increase simultaneously both of the ductility and strength of Al–Li 8090 alloy. Also, according to the performed finite element based thermal stress analysis, it is observed that a uniform distribution and high volume fraction of strengthening δ' (Al_3Li) precipitates are acquired via the directional quenching technique.

Keywords Aluminum–Lithium alloys · Ductility · Fractography · Aging heat treatment · δ' precipitates

1 Introduction

In the last two decades, various new composite materials and alloys have been fabricated for using in high technological industries [1–15]. One of them is Al–Li alloy which was used for the first time in aerospace structures with a view to reduce their weight. Recently, these alloys have been employed in cryogenic applications such as hydrogen and oxygen fuel tanks in aerospace vehicles [16]. Among various grades of Al–Li alloys, only in the Al–Li 8090 alloy, the second element after aluminum is lithium, while in other, the second element is copper. This issue leads to decrease the mass density of Al–Li 8090 alloy.

In recent years, several studies have been carried out to investigate different applications and characterizations of Al–Li 8090 alloy. Engler and Lucke [17] studied the texture development in the Al–Li 8090 alloy during cold rolling with the aid of X-ray pole figures and orientation distribution function analysis. Watkinson and Martin [18] correlated the changes in hardness of the duplex aged Al–Li 8090 alloy using transmission electron microscopy and differential scanning calorimetry. Kornisarov et al. [19] investigated the microstructure of the precipitates in an Al–Li 8090 alloy qualitatively and quantitatively by techniques of transmission electron microscopy through the stages of retrogression and reaging. Perez-Landazabal [20] employed the relative method to X-ray spectra in order to examine the precipitated mass fraction of δ and δ' in Al–Li alloys. Eddahbi et al. [21] analyzed the dynamic recrystallization of an Al–Li 8090 alloy at high temperatures and a specific value of the strain rate. Gaber and Afify [22] utilized the variation of thermophysical properties of Al–Li 8090 quenched from the solid solution state to indicate the temperatures at which the phase transformations occur. Bairwa and Date [23] determined tensile properties of Al–Li alloy sheets for three different

✉ S. Sahmani
ssahmani@nri.ac.ir

1 Mechanical Rotating Equipment Department, Niroo Research Institute (NRI), Tehran 16656-517, Iran

2 Materials Engineering Department, University of Tarbiat Modares, Tehran 14115-111, Iran

3 Metallurgy and Materials Engineering Department, Iran University of Science and Technology, Tehran 16846-13114, Iran

solutionising temperatures, with three ageing times at each of the three ageing temperatures. Kumaran et al. [24] identified the local maximum transition temperatures at the selected heating rate, precipitation of coherent δ', dissolution of δ' and precipitation of stable S′ and δ. They also studied the first differential of temperature dependent ultrasonic parameters as an effective tool to identify precipitation reactions in a slow-treated Al–Li 8090 alloy [25]. Katsikis et al. [26] investigated the microstructural stability during low temperature exposure of Al–Li 8090 alloys. Rajendran et al. [27] performed ultrasonic velocity and attenuation measurements on the as-received and thermally treated Al–Li 8090 alloys. Zhang et al. [28] explored the microstructure, electrical conductivity and mechanical properties of cast Al–2Li–2Cu–0.5 Mg–0.2Zr alloy during heat treatment. El-Aty et al. [29] reported the influence of sample orientation and strain rates on the tensile properties and anisotropy behavior of Al–Li alloys sheet through quasi-static and dynamic uniaxial tensile tests. Zhang et al. [30] anticipated the effect of creep aging on strength and toughness and microstructure evolution of Al–Li alloy using tensile test and Kahn tear test at room temperature, in conjunction with fractograph and transmission microstructure analysis. Liu et al. [31] studied the influences of surface abrasion on microstructure and pitting corrosion of Al–Li alloys.

During the aging heat treatment, the formation of the metastable phase $\delta'(Al_3Li)$ plays an essential role in the strengthening of the Al–Li 8090 alloy. In other words, the δ' precipitation has a long-range ordering structure which causes a significant effect on the slip procedure. Consequently, it yields to control the mechanism of dislocation breakdown. Various thermal treatments have been utilized to improve mechanical properties of different alloys such as Al–Li 8090 alloy. Gable et al. [32] predicted the quench sensitivity of Al–Li 8090 alloy via employing different coating rates from the solution heat treatment temperature. Kim et al. [33] enhanced the microhardness of a heat treated Al–Li 8090 alloy by increasing Mg content due to increased solid solution strengthening and reduction of the grain size. Nayan et al. [34] explored the hot deformation behavior of Al–Li alloys in homogenized condition via the hot isothermal compression testing. Rodak et al. [35] produced an ultrafine grained structure based on Al–Li alloys in the solution treated condition and additionally in aging condition.

The main problem in most aging heat treatments is the reduction of the ductility together with the enhancement of the strength. For instance, the thermomechanical aging heat treatments decrease significantly the ductility and make anisotropic properties. In the current study, a new heat treatment method namely as directional quenching is proposed which has the capability to increase simultaneously both of the ductility and strength of Al–Li 8090 alloy.

2 Experimental Procedure

2.1 Specimen

In the present study, a sheet of 2 mm thickness made of Al–Li 8090 alloy with chemical composition given in Table 1 is considered as the starting material. The main impurities are 0.05% Fe, 0.03% Si, 0.02% Ti, and 0.02% Zn (wt%). Two groups of specimen are manufactured. The first group includes small specimen with dimension 10 mm × 10 mm × 2 mm for using in the hardness test with standard number of ASTM E45. The second group includes tensile specimen with standard number of ASTM E8 to utilize in the tensile properties test.

2.2 Applied Aging Heat Treatments

Three different aging heat treatments are employed in this work to improve the mechanical properties of Al–Li 8090 specimen as below

(a) T6 → Solution treatment at 535 °C for 1 h + quenching within 0 °C water + aging at 170 °C for various times
(b) T8 (thermomechanical heat treatment) → Solution treatment at 535 °C for 1 h + quenching within 0 °C water + 14% cold rolling + aging at 170 °C for various times
(c) Directional quenching (the proposed method) → Solutionizing treatment along a specific direction at 535 °C for 1 h + quenching along a specific direction within 0 °C water + aging at 170 °C for various times

The proposed directional quenching method is similar to T6 heat treatment process. However, in this new method, heating and cooling process are conducted in a specific one direction. For this purpose, the specimen inserted in a castable alumina as the insulator in such a way that only one of six faces of the specimen is exposed to quenching. This procedure is depicted schematically in Fig. 1.

2.3 Microscopic Examinations

2.3.1 TEM

In order to perform the associated microstructural examinations, a Jeol, JEM microscope 2000FX operated at 200 kV is put to use. Thin discs of 2 mm diameter are punched from the prepared foils and then they are electro-polished via a twin jet device using a solution comprising 25% nitric acid and 75% methanol cooled to − 25 °C.

Table 1 Chemical composition of used Al–Li 8090 alloy

Element	Li	Cu	Mg	Zr	Impurities
wt%	2.48	1.51	1.15	0.10	≤ 0.15

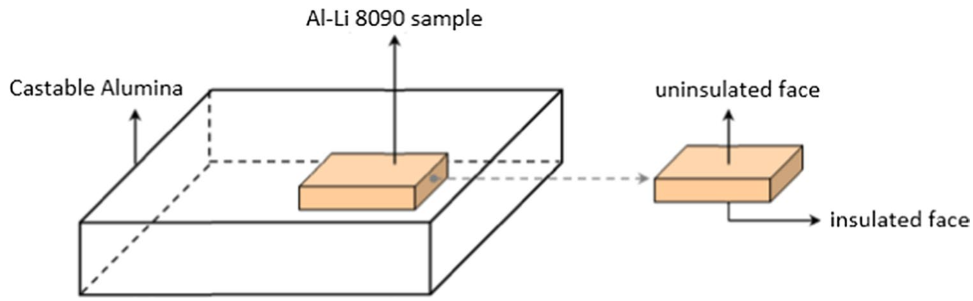

Fig. 1 Schematically representation of an inserted sample in a castable alumina as the insulator

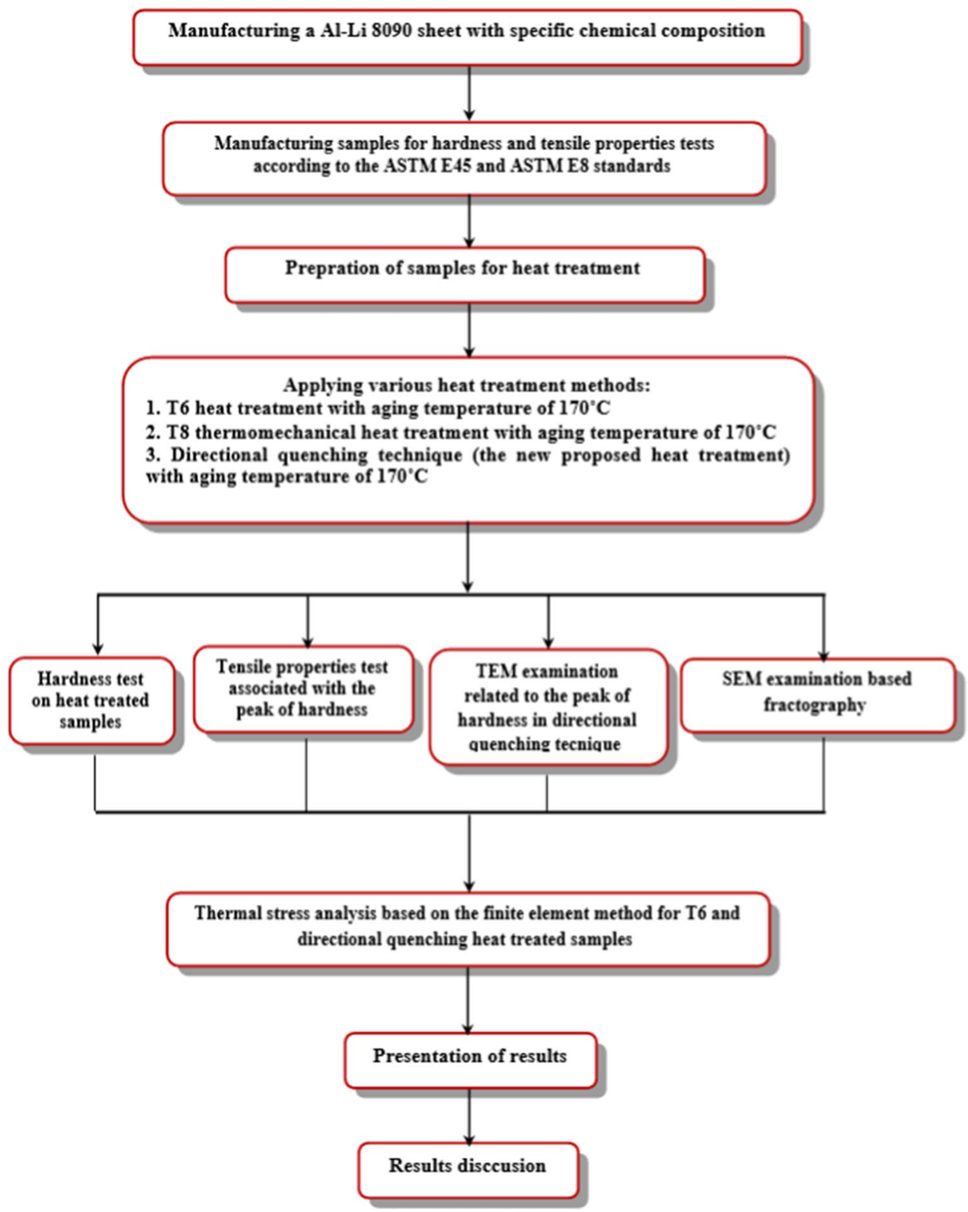

Fig. 2 Flowchart of the experimental procedure

2.3.2 SEM

PHILIPS XL-30 scanning electron microscope (SEM) is utilized for fractography analyses of specimen.

2.4 Mechanical Properties

The Brinell hardness test of 31.35 kg loading in accordance with ASTM E45 standard number, and tensile property

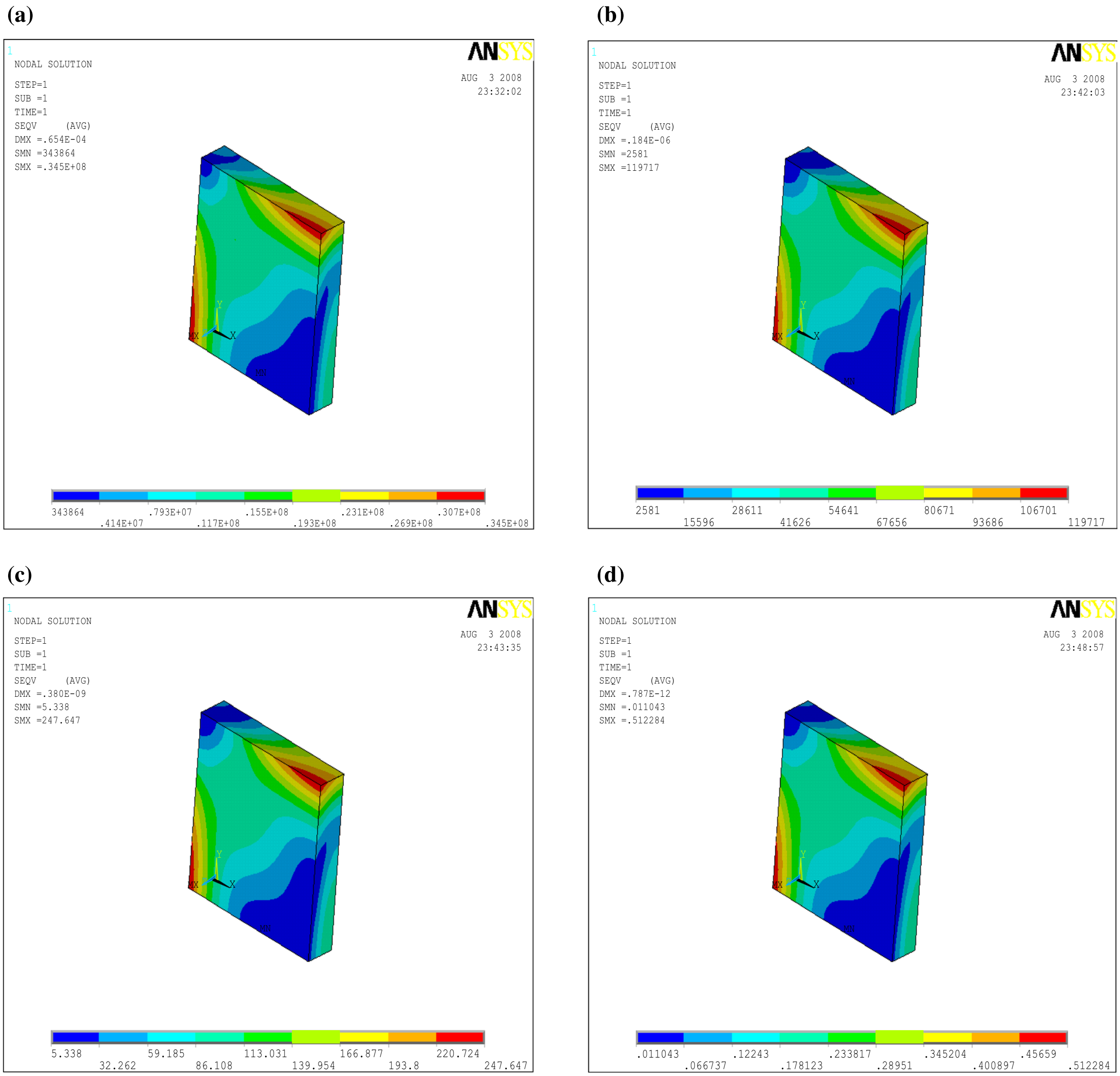

Fig. 3 Thermal stress analysis for a heat treated sample via T6 method after various times **a** $t = 0.25$ s, **b** $t = 5$ s, **c** $t = 10$ s, **d** $t = 15$ s

test with ASTM E8 standard number are performed on the related specimen.

2.5 Thermal Stress Analysis

In order to study the thermal gradients and thermoelastic stress distribution in specimen due to the quenching process, the finite element method via ANSYS software is employed.

The flowchart including all of the processes is depicted in Fig. 2.

3 Results and Discussion

3.1 Thermal Stress Analysis

The results of the thermal stress analyses using finite element method which are demonstrated the distribution of thermoelastic stress are presented in Figs. 3 and 4 corresponding to T6 and directional quenching methods, respectively. It is observed that the value of thermoelastic stress

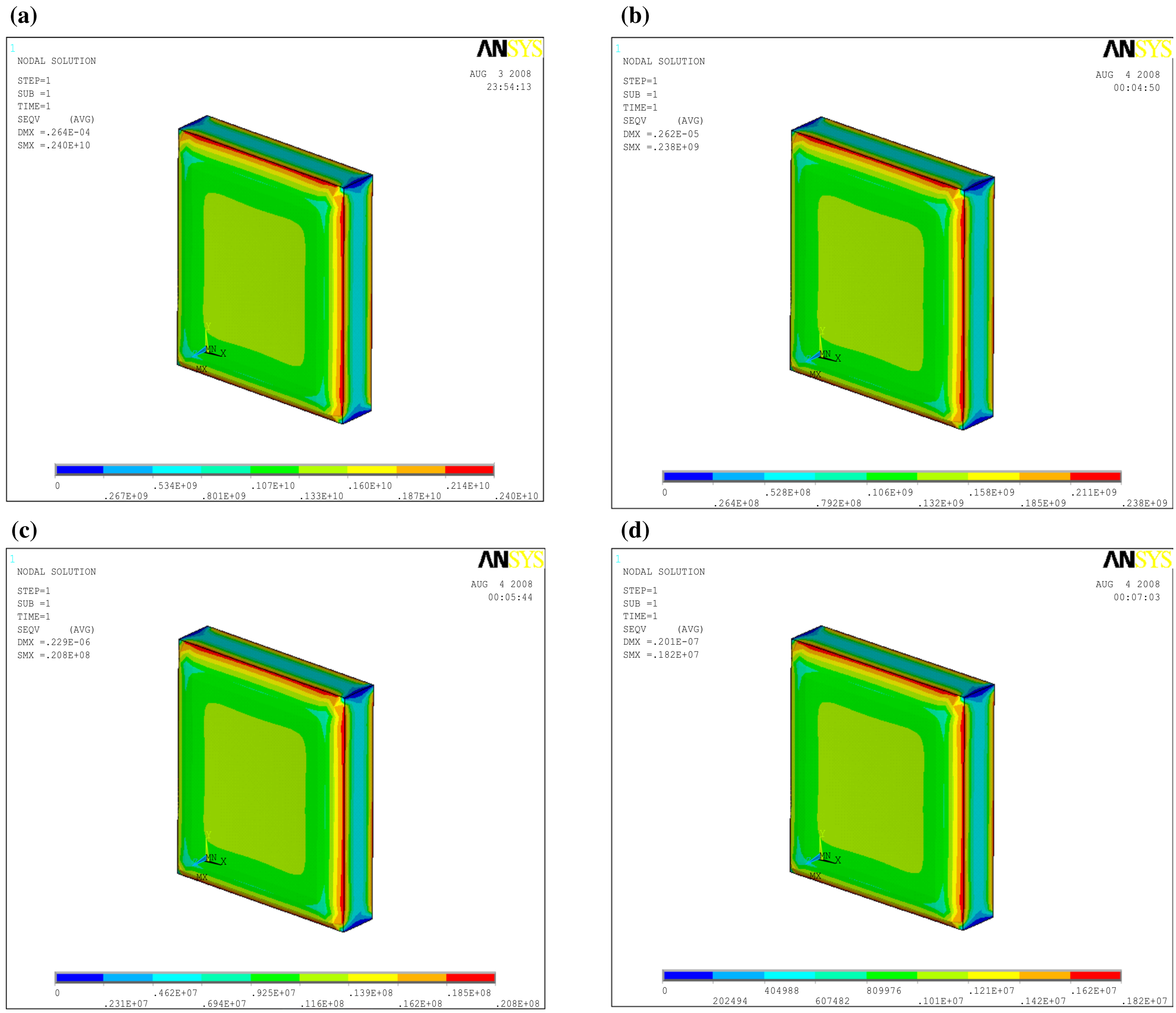

Fig. 4 Thermal stress analysis for a heat treated sample via directional quenching method after various times **a** $t=0.25$ s, **b** $t=5$ s, **c** $t=10$ s, **d** $t=15$ s

associated with the directional quenching is so higher and is distributed more uniformly compared to the T6 counterpart.

The high thermoelastic stress with uniform distribution obtained by the directional quenching method leads to nucleation and growth of δ' fine phase which results into improve simultaneously both of the strength and ductility of specimen. In Fig. 5a, the TEM microstructure of a heat treated sample via the directional quenching method is shown. The uniform distribution of the δ' fine phase can be seen clearly. It is indicated that the diameter of these δ' spherical precipitates is within the range of 4–24 nm. Also, In Fig. 5b, the selected area diffraction pattern (SADP) associated with the δ' spherical precipitates is illustrated. According to the SADP along [1 1 0] direction, it is obvious that the structure of these precipitates is an ordered $L1_2$.

3.2 Hardness Property

In Fig. 6, the variation of hardness with time corresponding to different aging heat treatments is illustrated. It can be seen that all of the plots represent the same pattern. At first, an increment in the value of hardness occurs up to a maximum point. Thereafter, the hardness of specimen reduces with time. The reason of the initial increment in the hardness is due to the creation of GP zones and intermediate precipitations which nucleate and grow coherently with the matrix. It should be noted that a more homogenous distribution of

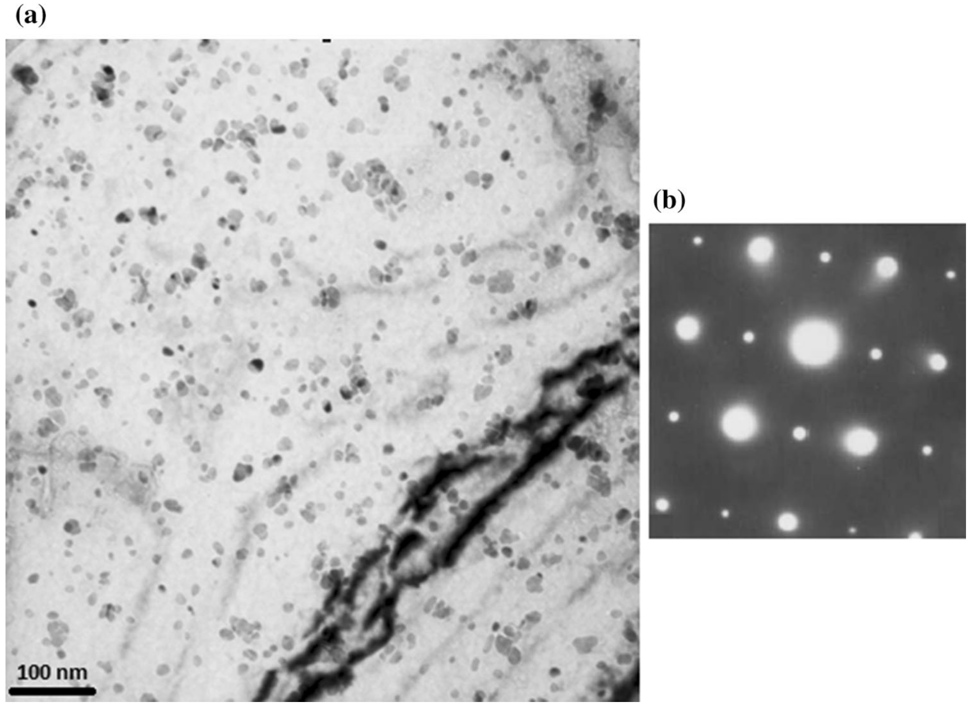

Fig. 5 **a** TEM image of a heat treated sample via the directional quenching method, **b** SADP associated with the δ' spherical precipitates along [1 1 0] direction

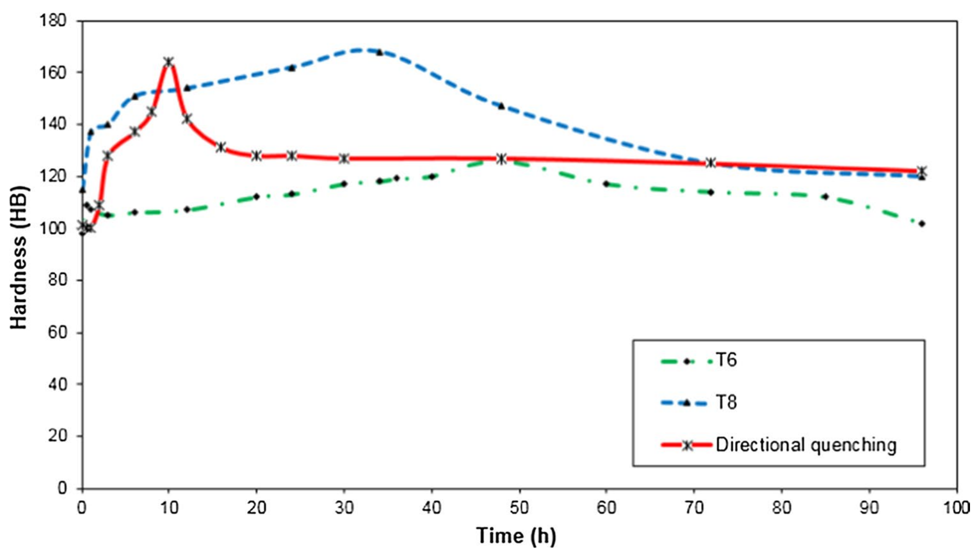

Fig. 6 Variation of hardness with time corresponding to different heat treatment techniques

Table 2 Tensile properties of non-heat treated sample

Yield stress (MPa)	Ultimate tensile strength (MPa)	Elongation (%)
127.65	276.82	11.04

Table 3 Tensile properties of heat treated specimen via T6 method with aging temperature of 170 °C

Aging Time (hr)	34	48	72
Yield Stress (MPa)	322.41	330.26	320.16
Ultimate Tensile Strength (MPa)	405.22	418.57	400.07
Elongation (%)	6.27	7.02	6.42

Table 4 Tensile properties of heat treated specimen via T8 method with aging temperature of 170 °C

Aging Time (hr)	1	3	6	12	24	34	48	72	96
Yield Stress (MPa)	296.15	388.14	497.61	511.07	513.80	521.63	485.20	380.12	312.05
Ultimate Tensile Strength (MPa)	325.71	415.71	537.28	545.16	552.47	558.85	504.17	406.71	330.37
Elongation (%)	4.68	3.94	3.17	3.27	4.15	4.21	3.82	3.91	4.73

Table 5 Tensile properties of heat treated specimen via directional quenching technique with aging temperature of 170 °C

Aging Time (hr)	8	10	12	48
Yield Stress (MPa)	388.35	424.80	379.16	335.03
Ultimate Tensile Strength (MPa)	458.27	520.50	447.89	438.81
Elongation (%)	9.28	10.18	9.47	10.02

these precipitations leads to enhance the hardness more efficiently. Through transformation of the intermediate precipitations to δ' (Al_3Li) coherent phase, the maximum hardness achieves. After this maximum point, by passing the aging time, the precipitations grow to a high level which causes to decrease the hardness.

Through comparison of the directional quenching and T6 heat treatment method, it is revealed that the value of the hardness at the maximum point associated with the direction quenching method is higher than that of the T6 one. Moreover, the needed time to obtain the maximum hardness decreases from 48 h in T6 method to 10 h in the directional quenching method. The reason of such improvements is the creation of high value of the thermos-elastic stress in the directional quenching method. This high stress acts as a driving force to create strengthening δ' (Al_3Li) precipitates in a more short time with higher volume fraction.

By comparing the results associated with the directional quenching and T8 heat treatment methods, it is found that the values of the hardness in the maximum points are approximately the same, but the needed time to acquire the maximum hardness reduces from 34 h in T8 method to 10 h in the directional quenching method. It means that the effect of thermos-elastic stress due to the directional quenching process on the atomic diffusion, nucleation and growth of δ' phase is more than that of the stress due to the cold work in T8 process.

3.3 Tensile Properties

In Tables 2, 3, 4 and 5, the yield strength, ultimate tensile strength, and elongation of a non-heat treated sample, T6, T8 and directional quenching heat treated samples are given. The results associated with the peak of hardness are presented in the highlighted column of the tables. In accordance with the presented results, in T6 and T8 heat treatment methods, the strength enhances, but the elongation decreases significantly compared to the non-heat treated sample. However, in the directional quenching method, the strength of the heat treated sample increases as well as the elongation is higher than that of T6 and T8 methods. The reason of this observation is uniform distribution of δ' phase as mentioned in the thermal stress analysis.

3.4 Fractography

In Figs. 7, 8 and 9, the SEM micrographs of cross-sectional fracture pattern at the time associated with the peak of hardness as well as before and after it are represented for samples which are heat treated with different heat treatment methods. For the heat treated sample with T6 method, an ununiformed distribution of ductility can be seen in the cross-sectional fracture pattern. For example, in Fig. 7b, a complete brittle fracture is observed at point A, but at point B, the type of fracture tends to a ductile one. This pattern is probably due to the ununiformed distribution of δ' phase during the T6 aging heat treatment.

For the heat treated sample with T8 method, a smooth cross-sectional fracture pattern is found which indicates a complete brittle fracture. However, for the heat treated sample with the directional quenching method, the presence of cavities with appropriate depth in the cross-sectional fracture pattern indicates a significant deformation of the sample during the fracture procedure. These cavities are distributed uniformly within the cross-sectional fracture pattern.

4 Conclusion

The main objective of this work was to introduce a new aging heat treatment method namely as the directional quenching technique to improve the mechanical properties of Al–Li 8090 alloy. To this end, the solutionizing treatment as well as quenching were conducted along a specific direction. In order to confirm the advantage of this

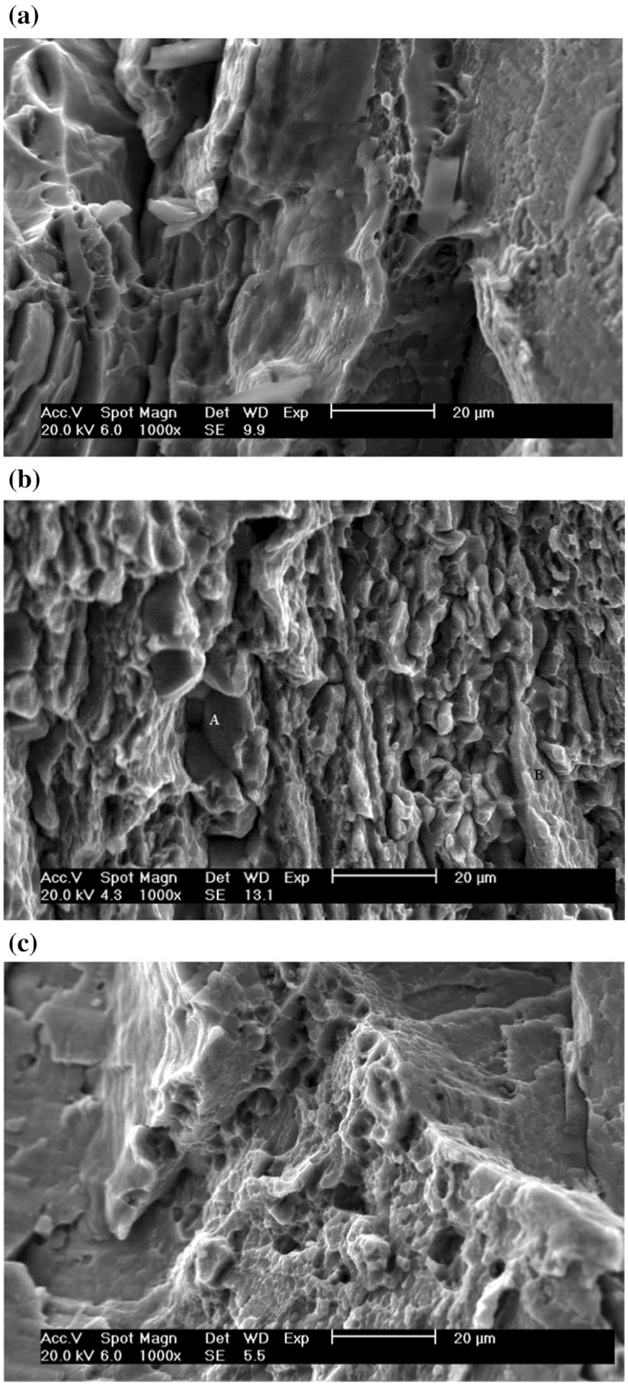

Fig. 7 SEM micrographs of cross-sectional fracture patterns corresponding to T6 heat treatment technique with aging temperature of 170 °C: **a** $t=34$ h, **b** $t=48$ h, **c** $t=72$ h

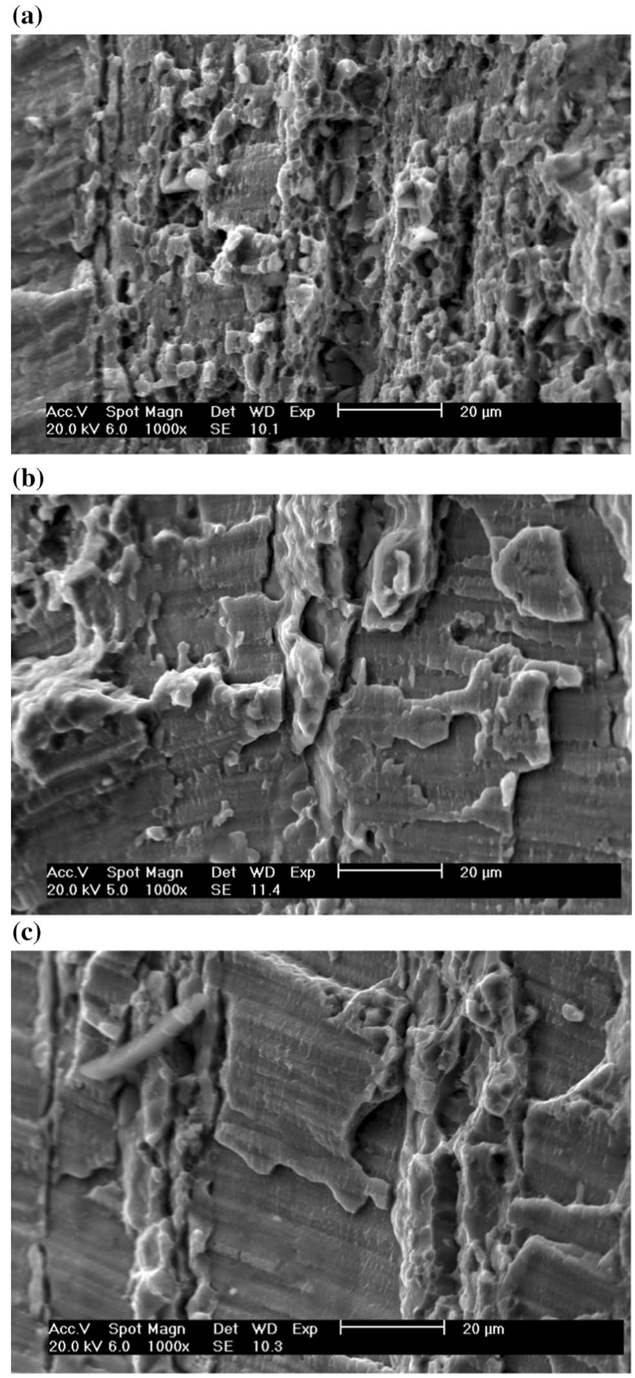

Fig. 8 SEM micrographs of cross-sectional fracture patterns corresponding to T8 heat treatment technique with aging temperature of 170 °C: **a** $t=6$ h, **b** $t=34$ h, **c** $t=72$ h

method, the results obtained from it were compared with those of T6 and T8 conventional heat treatment methods. It was observed that in opposite to the two other methods, the directional quenching technique has the capability to enhance simultaneously both of the strength and ductility of Al–Li 8090 alloy. Moreover, based upon the conducted finite element based thermal stress analysis, it was demonstrated that there is a uniform distribution with

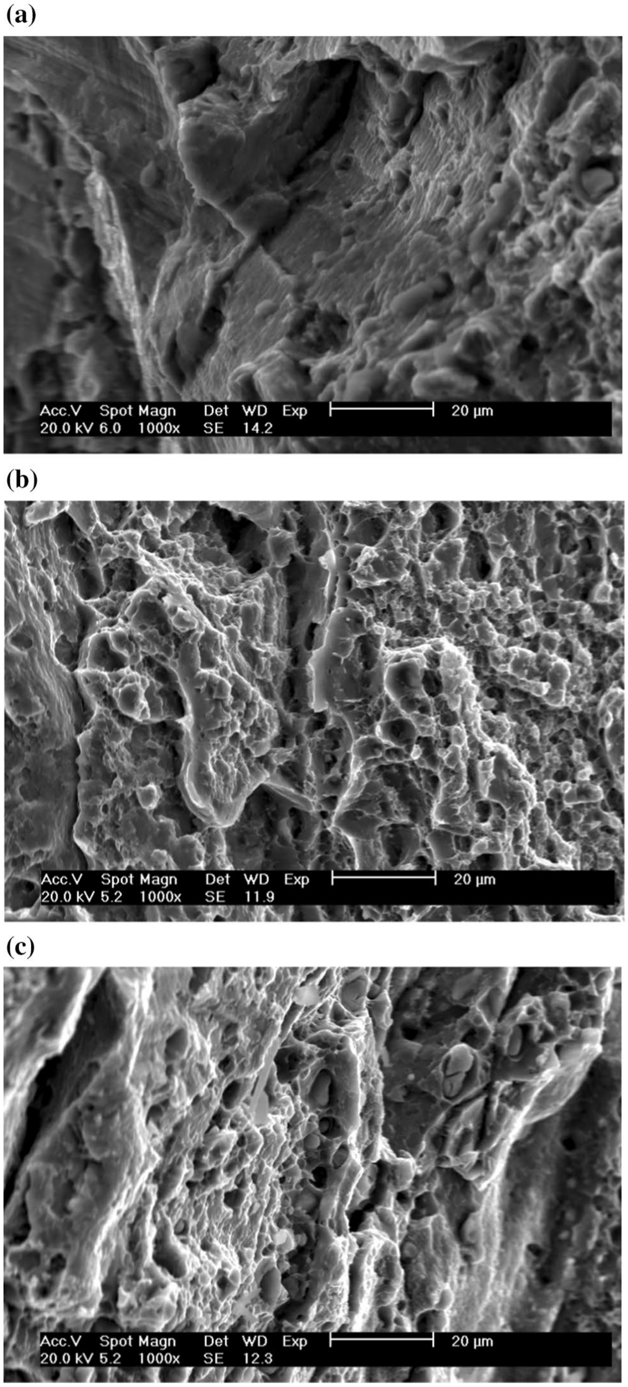

Fig. 9 SEM micrographs of cross-sectional fracture patterns corresponding to directional quenching heat treatment technique with aging temperature of 170 °C: **a** $t = 8$ h, **b** $t = 10$ h, **c** $t = 12$ h

high volume fraction of δ' (Al_3Li) precipitates within the improved heat treated sample via the directional quenching method.

Data availability The raw/processed data required to reproduce these findings cannot be shared at this time due to legal or ethical reasons.

References

1. J.S. Suh, D. Klaumunzer, H.S. Kim, Y.M. Kim, B.S. You, Microstructures and mechanical properties of direct-extruded novel Mg alloys. Procedia Eng. **207**, 908–913 (2017)
2. S. Sahmani, A. Khandan, S. Saber-Samandari, M.M. Aghdam, Nonlinear bending and instability analysis of bioceramics composed with magnetite nanoparticles: Fabrication, characterization, and simulation. Ceram. Int. **44**, 9540–9549 (2018)
3. Y. Yang, L. Wang, L. Snead, S.J. Zinkle, Development of novel Cu-Cr-Nb-Zr alloys with the aid of computational thermodynamics. Mater. Des. **156**, 370–380 (2018)
4. S. Sahmani, M.M. Aghdam, T. Rabczuk, A unified nonlocal strain gradient plate model for nonlinear axial instability of functionally graded porous micro/nano-plates reinforced with graphene platelets. Mater. Res. Express **5**, 045048 (2018)
5. E. Chicardi, C. Aguilar, M.J. Sayagues, C. Garcia, Influence of the Mn content on the TiNb*x*Mn alloys with a novel fcc structure. J. Alloys Compd. **746**, 601–610 (2018)
6. J. Lu, Y. Zhao, Y. Du, W. Zhang, Y. Zhang, Microstructure and mechanical properties of a novel titanium alloy with homogeneous $(TiHf)_5Si_3$ article-reinforcements. J. Alloy. Compd. **778**, 115–123 (2019)
7. S. Sahmani, S. Saber-Samandari, M.M. Aghdam, A. Khandan, Nonlinear resonance response of porous beam-type implants corresponding to various morphology shapes for bone tissue engineering applications. J. Mater. Eng. Perform. **27**, 5370–5383 (2018)
8. P. Sotoudehbagha, S. Sheibani, M. Khakbiz, S. Ebrahimi-Barough, H. Hermawan, Novel antibacterial biodegradable Fe–Mn–Ag alloys produced by mechanical alloying. Mater. Sci. Eng. C **88**, 88–94 (2018)
9. S. Sahmani, S. Saber-Samandari, A. Khandan, M.M. Aghdam, Nonlinear resonance investigation of nanoclay based bio-nanocomposite scaffolds with enhanced properties for bone substitute applications. J. Alloys Compd. **773**, 636–653 (2019)
10. J. Ren, Z. Chen, J. Peng, W. Ma, S.P. Ringer, An initial report on achieving high comprehensive performance in an Al–Mg–Si alloy via novel thermomechanical processing. J. Alloys Compd. **764**, 679–683 (2018)
11. S. Sahmani, M. Shahali, A. Khandan, S. Saber-Samandari, M.M. Aghdam, Analytical and experimental analyses for mechanical and biological characteristics of novel nanoclay bio-nanocomposite scaffolds fabricated via space holder technique. Appl. Clay Sci. **165**, 112–123 (2018)
12. Q. Jia, P. Rometsch, S. Cao, K. Zhang, X. Wu, Towards a high strength aluminium alloy development methodology for selective laser melting. Mater. Des. **174**, 107775 (2019)
13. S. Sahmani, S. Saber-Samandari, A. Khandan, M.M. Aghdam, Influence of MgO nanoparticles on the mechanical properties of coated hydroxyapatite nanocomposite scaffolds produced via space holder technique: Fabrication, characterization and simulation. J. Mech. Behav. Biomed. Mater. **95**, 76–88 (2019)
14. Y. Yang, X. Lian, K. Zhou, G. Li, Effects of laser shock peening on microstructures and properties of 2195 Al–Li alloy. J. Alloys Compd. **781**, 330–336 (2019)
15. S. Sahmani, M. Shahali, M. Ghadirinejad, A. Khandan, M.M. Aghdam, S. Saber-Samandari, Effect of copper oxide nanoparticles on electrical conductivity and cell viability of calcium phosphate scaffolds with improved mechanical strength for bone tissue engineering. Eur. Phys. J. Plus **134**, 7 (2019)
16. A.A. El-Aty, Y. Xu, X. Guo, S.-H. Zhang, D. Chen, Strengthening mechanisms, deformation behavior, and anisotropic mechanical properties of Al–Li alloys: a review. J. Adv. Res. **10**, 49–67 (2018)

17. O. Engler, K. Lucke, Influence of the precipitation state on the cold rolling texture in 8090 Al–Li material. Mater. Sci. Eng. A **148**, 15–23 (1991)
18. P.C. Watkinson, J.W. Martin, δ'-Phase precipitation at low temperature in a duplex-aged 8090 Al–Li alloy. Mater. Charact. **33**, 11–19 (1994)
19. V. Komisarov, M. Talianker, B. Cina, Effect of retrogression and reaging on the precipitates in an 8090 Al–Li alloy. Mater. Sci. Eng. A **242**, 39–49 (1998)
20. J.I. Pérez-Landazábal, M.L. Nó, G. Madariaga, V. Recarte, J. San Juan, Quantitative analysis of δ' precipitation kinetics in Al–Li alloys. Acta Materialia **48**, 1283–1296 (2000)
21. M. Eddahbi, C.B. Thomson, F. Carrerio, O.A. Ruano, Grain structure and microtexture after high temperature deformation of an Al–Li (8090) alloy. Mater. Sci. Eng. A **284**, 292–300 (2000)
22. A. Gaber, N. Afify, Characterization of the precipitates in Al–Li(8090) alloy using thermal measurements and TEM examinations. Physica B **315**, 1–6 (2002)
23. M.L. Bairwa, P.P. Date, Effect of heat treatment on the tensile properties of Al–Li alloys. J. Mater. Process. Technol. **153–154**, 603–607 (2004)
24. S. Muthu Kumaran, N. Priyadharsini, V. Rajendran, T. Jayakumar, B. Raj, In situ high temperature ultrasonic evaluation for on-line characterisation of fine scale precipitation reactions in 8090 Al–Li alloy. Mater. Sci. Eng. A **435–436**, 29–39 (2006)
25. S. Muthu Kumaran, V. Rajendran, T. Jayakumar, P. Palanichamy, B. Raj, First differential of temperature dependent ultrasonic parameters as an effective tool for identifying precipitation reactions in a slow heat-treated 8090 Al–Li alloy. J. Alloys Compd. **464**, 150–156 (2008)
26. S. Katsikis, B. Noble, S.J. Harris, Microstructural stability during low temperature exposure of alloys within the Al–Li–Cu–Mg system. Mater. Sci. Eng. A **485**, 613–620 (2008)
27. V. Rajendran, S. Muthu-Kumaran, T. Jayakumar, P. Palanichamy et al., Microstructure and ultrasonic behaviour on thermal heat-treated Al–Li 8090 alloy. J. Alloys Compd. **478**, 147–153 (2009)
28. X. Zhang, L. Zhang, G. Wu, W. Liu, J. Sun, Microstructural evolution and mechanical properties of cast Al–2Li–2Cu–0.5 Mg–0.2Zr alloy during heat treatment. Mater. Charact. **132**, 312–319 (2017)
29. A.A. El-Aty, Y. Xu, S. Zhang, Y. Ma, D. Chen, Experimental investigation of tensile properties and anisotropy of 1420, 8090 and 2060 Al-Li alloys sheet undergoing different strain rates and fibre orientation: a comparative study. Procedia Eng. **207**, 13–18 (2017)
30. J. Zhang, C. Wang, Y. Zhang, Y. Deng, Effects of creep aging upon Al–Cu–Li alloy: Strength, toughness and microstructure. J. Alloys Compd. **764**, 452–459 (2018)
31. J. Liu, K. Zhao, M. Yu, S. Li, Effect of surface abrasion on pitting corrosion of Al–Li alloy. Corros. Sci. **138**, 75–84 (2018)
32. B.M. Gable, A.A. Csontos, E.A. Starke Jr., A quench sensitivity study on the novel Al–Li–Cu–X alloy AF/C 458. J. Light Met. **2**, 65–75 (2002)
33. J.-M. Kim, K.-D. Seong, J.-H. Jun, K. Shin, K.-T. Kim, W.-J. Jung, Microstructural characteristics and mechanical properties of Al–2.5 wt% Li–1.2 wt% Cu–*x*Mg alloys. J. Alloys Compd. **434–435**, 324–326 (2007)
34. N. Nayan, S.V.S. Narayana Murty, S. Chhangani, A. Prakash, M.J.N.V. Prasad, I. Samajdar, Effect of temperature and strain rate on hot deformation behavior and microstructure of Al–Cu–Li alloy. J. Alloys Compd. **723**, 548–558 (2017)
35. K. Rodak, A. Urbancyzk-Gucwa, M. Jabloriska, J. Pawlicki, J. Mizera, Influence of heat treatment on the formation of ultrafine-grained structure of Al–Li alloys processed by SPD. Arch. Civ. Mech. Eng. **18**, 331–337 (2018)